Materials Chemistry and Physics 247 (2020) 122881

Contents lists available at ScienceDirect

Materials Chemistry and Physics

journal homepage: www.elsevier.com/locate/matchemphys

PANI-Fe_2O_3 composite for enhancement of active life of alkyd resin coating for corrosion protection of steel

V.S. Sumi [a], S.R. Arunima [a], M.J. Deepa [a], M. Ameen Sha [a], A.H. Riyas [a], M.S. Meera [a], Viswanathan S. Saji [b], S.M.A. Shibli [a,*]

[a] Department of Chemistry, University of Kerala, Kariavattom Campus, Thiruvananthapuram, Kerala, 695 581, India
[b] Center of Research Excellence in Corrosion, Research Institute, King Fahd University of Petroleum & Minerals, Dhahran, 31261, Saudi Arabia

HIGHLIGHTS

- PANI-Fe_2O_3 composite was synthesized and incorporated into a commercial alkyd resin.
- Anticorrosive coating on mild steel was developed by dip coating.
- Assimilation of PANI-Fe_2O_3 composite significantly improved the corrosion resistance of alkyd coating.
- The enhancement was attributed to the higher passivation ability and the filler effect of PANI-Fe_2O_3.

GRAPHICAL ABSTRACT

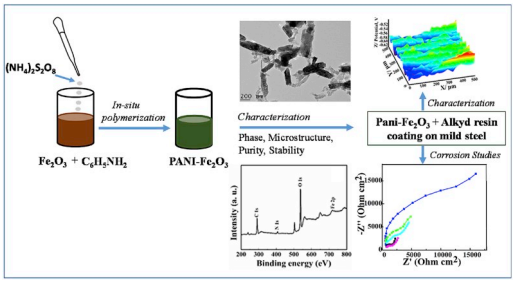

ARTICLE INFO

Keywords:
Surface coating
Alkyd resin
PANI-Fe_2O_3
Nanocomposite
Corrosion protection

ABSTRACT

In-situ synthesized PANI-Fe_2O_3 composite was incorporated into a commercial alkyd resin and developed an efficient anticorrosive coating for mild steel. Both the composite and the fabricated alkyd resin coating were systematically characterized by using FTIR, XRD, SEM, TEM, XPS, TGA, OSP, SKPM, and EDS. Corrosion-resistant characteristics of the nanocomposite coatings were evaluated by potentiodynamic polarization, impedance spectroscopy, and long-term open circuit potential measurements in 3.5% NaCl and 1 M HCl. The much-improved corrosion resistance of the PANI-Fe_2O_3 incorporated coating was correlated with the better barrier performance and the passivation protection offered. The higher corrosion resistance observed in the acidic medium was explained by the complimentary cathodic reaction of the conductive emeraldine-PANI to the nonconductive leuco-PANI. The fabrication method provided can be beneficial for developing eco-friendly anticorrosion 'conducting polymer-metal oxide-alkyd resin' coatings.

1. Introduction

Organic coatings are the most effective and widely employed method for corrosion prevention [1,2]. Among the different organic coatings, alkyd resins are attractive due to their excellent properties such as superior rigidity, mechanical strength, high adhesion strength, good thermal stability and easy processing routes [3–5]. One disadvantage of the alkyd coatings is their inherent brittleness [6,7]. In this direction, many research efforts are put forward to fabricate novel organic-inorganic nanocomposite alkyd coatings [8–12].

* Corresponding author.
E-mail address: smashibli@yahoo.com (S.M.A. Shibli).

https://doi.org/10.1016/j.matchemphys.2020.122881
Received 2 September 2019; Received in revised form 6 February 2020; Accepted 2 March 2020
Available online 5 March 2020
0254-0584/

Conducting polymer coatings are another group of organic coatings that received extensive research attention as an environmentally friendly coating with both physical and electronic barrier effect [13–16]. Conducting polymer coatings are more tolerant of pin-holes and scratches due to their passivation ability [17–20]. Polyaniline (PANI), is a commonly employed conducting polymer due to its high thermal stability, ease of synthesis and high electrochemical activity [21]. In the doped and conducting state, they can protect steel from corrosion by an anodic mechanism via the production and regeneration of an iron oxide layer at the interface [22–24]. The major disadvantage with the PANI coating is perhaps the inferior interfacial addition [25, 26]. Among the different methods adopted for enhancing the adhesion and abrasion resistance, the formulation of PANI-based nanocomposite coating is a practical approach [27,28].

Several recent works are available on conducting polymer-based nanocomposite coatings for steel. Karpakam et al. reported that PANI-molybdate coating exhibited high corrosion protection than pure PANI coating due to the additional passivating ability of molybdate ions [29]. Radhakrishnan et al. reported that PANI-TiO_2 synthesized by an *in situ* polymerization showed excellent corrosion resistance for steel [30]. Shi et al. reported a PANI-SiO_2 composite coating for active corrosion protection of Mg–Li alloy [31]. Studies have shown that the presence of reduced graphene oxide promoted the passivation ability of PANI and the composite coating effectively protected Al alloy from corrosion [32]. A few studies have shown that PANI-Fe_2O_3 composites offer excellent corrosion protection [33,34].

Fe_2O_3 has several advantages. It exhibits semiconducting properties and is extensively used in electrode materials and gas sensing applications due to the high corrosion resistance characteristics. Fe_2O_3 is attractive in terms of cost and availability and can function as an effective filler enhancing the adhesion, abrasion resistance and mechanical properties of PANI [35–37]. The excellent features, such as good dispersion and hydrophobicity make them an attractive candidate [38–40]. A PANI-Fe_2O_3 coating can provide enhanced barrier properties and passivation protection, coupled with both conducting and ferromagnetic properties [33,34].

A few studies reported that corrosion resistance of the traditional alkyd and epoxy-based resins could be improved by the addition of PANI [6,23,41,42]. Chen et al. revealed a PANI-epoxy resin coating that offered excellent anti-corrosion to mild steel in 3.5% NaCl solution [42]. Goncalves et al. investigated the performance of alkyd paints containing PANI derivatives for the protection of carbon steel [23].

In this context, we planned to study a PANI-Fe_2O_3-alkyd coating for mild steel. An *in situ* polymerization method was used for PANI-Fe_2O_3 synthesis, and the composite was subsequently assimilated to the alkyd coating. To the best of our knowledge, no studies have dedicated to seeing the effect of the addition of PANI-Fe_2O_3 composite to an alkyd resin coating. Detailed studies were performed in characterizing the *in situ* synthesized PANI-Fe_2O_3 composite and evaluating the corrosion resistance of the composite-incorporated alkyd coating.

2. Experimental

2.1. Chemicals

Aniline, iron(III) chloride hexahydrate, ammonium persulphate, phosphoric acid, hydrochloric acid and sodium chloride were purchased from Merck®. All the reagents were of analytical grade. Aniline was used after vacuum distillation.

2.2. Preparation and characterization of PANI-Fe_2O_3 composite

For the synthesis of the PANI-Fe_2O_3 composite, 1 M distilled aniline was dissolved in phosphoric acid, then Fe_2O_3 was added and stirred well. Pre-cooled ammonium persulfate ($(NH_4)_2S_2O_8$ as an oxidizing agent) was added drop-wise to the pre-cooled aniline-Fe_2O_3 mixture for about 1.5 h with constant stirring. To ensure the complete polymerization, stirring was continued for 2 h. A dark green coloured PANI-Fe_2O_3 composite thus formed was filtered and repeatedly washed with distilled water to remove excess acid content. The polymer composite was dried in a hot-air oven at 80 °C for 2 h. The dried PANI-Fe_2O_3 composite was finely ground and then used as a pigment for the coating.

The diffraction pattern of the composite was obtained by an X-ray diffractometer (XRD, Shimadzu–6000) with Cu Kα radiation (current - 30 mA, 2°/min, step size 0.02°). Fourier transform infrared spectroscopy (FTIR) analysis of the synthesized composite was carried out by Thermo Nicolet, Avatar 370 spectrometer. The vibrational modes of the composites were studied in the mid-IR region from 350 to 4000 cm^{-1} with KBr pellet using a diffused reflectance spectroscopic technique. The size and morphology of the synthesized PANI-Fe_2O_3 composite were analyzed by Field Emission Scanning Electron Microscopy (FESEM, Nova Nano 450 with FESEM Bruker) and Transmission Electron Microscopy (TEM, JEOL JEM-2100). The PANI-Fe_2O_3 composite was further characterized by X-ray Photoelectron Spectroscopy (XPS, Thermoscientific ESCALAB 250) with an exciting source of Al Kα radiation. The thermal behavior of the composite was studied by Thermogravimetric Analysis (TGA, PerkinElmer, STA 8000). A heating rate of 35 °C/min. Was used.

2.3. Preparation and characterization of PANI-Fe_2O_3/alkyd resin coating

The PANI-Fe_2O_3 composite-incorporated alkyd resin coatings were developed on mild steel substrate by dip coating (repeated three times). Here, five coating formulations were prepared by adding 0, 0.01, 0.02, 0.05 and 0.1 g each of PANI-Fe_2O_3 composite to a mixed solution of 5 mL each of xylene and alkyd resin and stirred for 10 h. The coated mild steel

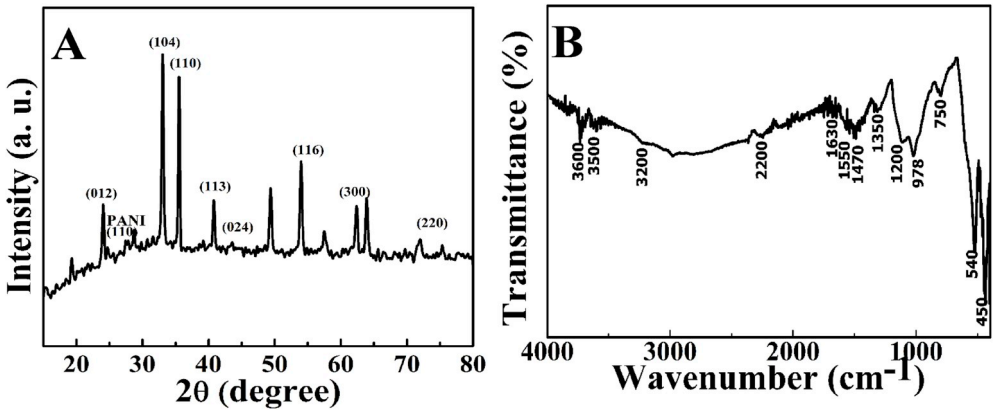

Fig. 1. (A) XRD and (B) FTIR absorption spectra of PANI-Fe_2O_3 composite.

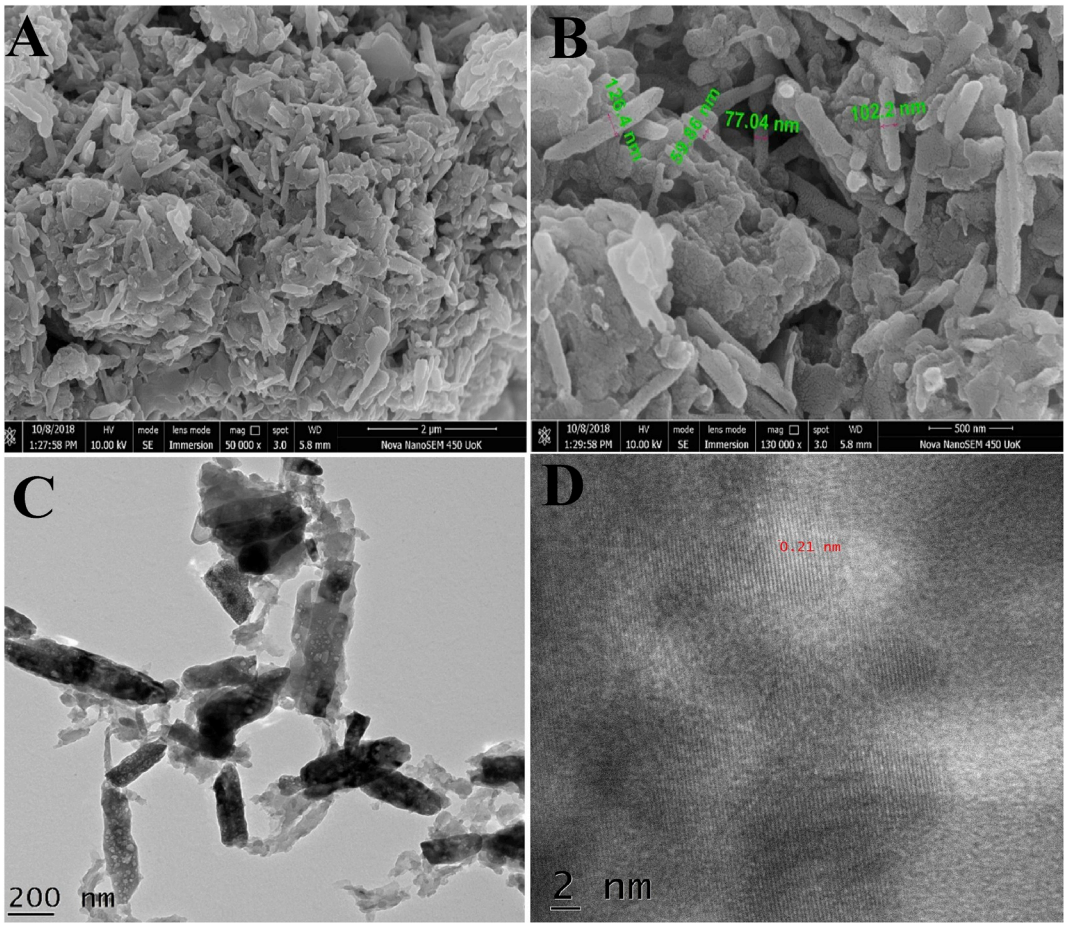

Fig. 2. FESEM images (A & B) and HRTEM images (C & D) of PANI-Fe_2O_3 composite at different magnifications.

samples were dried at room temperature overnight. The developed coatings were represented as bare alkyd resin, PANI-Fe_2O_3 1(g/L)/alkyd resin, PANI-Fe_2O_3 2(g/L)/alkyd resin, PANI-Fe_2O_3 5(g/L)/alkyd resin and PANI-Fe_2O_3 10(g/L)/alkyd resin respectively for 0, 0.01, 0.02, 0.05 and 0.1 g of PANI-Fe_2O_3 composite added to 10 mL mixed solution of xylene and alkyd resin.

The surface topography and coating stability were evaluated by using Optical Surface Profilometry (OSP) and Scanning Kelvin Probe Microscopy (SKPM, M370 scanning electrochemical workstation, Uniscan, UK). SEM/Energy Dispersive Spectroscopy (SEM/EDS, JEOL JSM - 840A) was used to study the surface morphology and composition of the coatings.

2.4. Electrochemical studies

Electrochemical corrosion studies of the developed coatings were performed using electrochemical work station (Biologic SP 200) with a typical three-electrode system where Ag/AgCl/saturated KCl, Pt and the coated mild steel were used as the reference, counter and working electrodes respectively. Studies were conducted in 3.5% NaCl and in 1 M HCl solutions. Electrochemical Impedance Spectroscopy (EIS) experiments were performed at the range of 10 mHz–100 kHz, after attaining a stable equilibrium potential in the respective electrolyte solution for an initial immersion period of 1 h. EC lab software was used. Long-term stability of the coatings was monitored by following open circuit potential (OCP) decay as a function of immersion time.

3. Results and discussion

3.1. Physicochemical characterization of PANI-Fe_2O_3 composite

The phase structure and crystallinity of the PANI-Fe_2O_3 composite was confirmed from XRD analysis. The XRD pattern of the synthesized PANI-Fe_2O_3 composite is shown in Fig. 1A. The broad diffraction peak centered at 25.3° could be attributed to (110) plane of PANI and that can be attributed to its amorphous nature [43,44]. The crystalline peaks appeared at 24.4°, 33.2°, 35.7°, 40.8°, 45.8°, 54.1°, 64.1°and 72.1° corresponds to (012), (104), (110), (113), (024), (116), (300) and (220) planes of hexagonal Fe_2O_3 (JCPDS 33–0664) [45–47]. The average crystallite size of the composite calculated using Scherrer formula ($D = 0.9\ \lambda/\beta\ \cos\theta$, where D is the average crystallite diameter, and β is full-width half maxima of the diffraction beam) was ~80 nm.

The FTIR spectrum of PANI-Fe_2O_3 composite is shown in Fig. 1B. The peak observed at 1630 cm^{-1} is attributed to C=C stretching vibrations of the quinoid ring and the peak at 1470 cm^{-1} to the C=C stretching vibrations of the benzenoid ring [48]. The peak at 1550 cm^{-1} could be ascribed to the characteristic band of the secondary amino group in the polymer chain [49], and the peak at 978 cm^{-1} is typical of the N–H stretching vibrations [50]. Meanwhile, the band at 1200 cm^{-1} is assigned to the stretching of the C–N bonds of the aromatic amines. The peak at 530 and 450 cm^{-1} corresponds to the bending mode of Fe–O. The peak at 3600 cm^{-1} corresponds to the water molecule associated with the metal oxide [51]. The characteristic peaks of both PANI and Fe_2O_3 found in the spectrum of the nanocomposite confirmed the successful incorporation of the metal oxide in the polymer matrix.

The SEM images of the composites (Fig. 2A&B) showed irregular rod-shaped Fe_2O_3 particles distributed unevenly in the PANI polymer

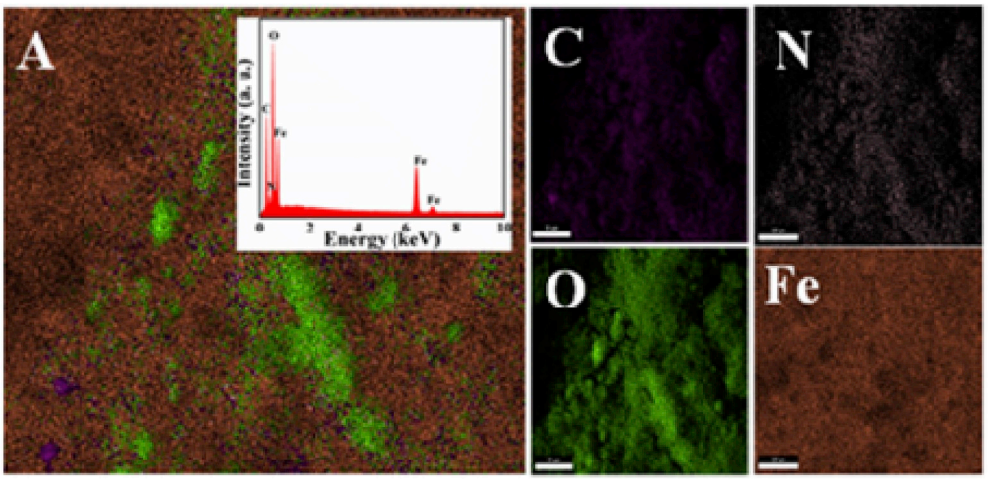

Fig. 3. EDS mapping of PANI-Fe_2O_3 composite (inset: EDS spectrum).

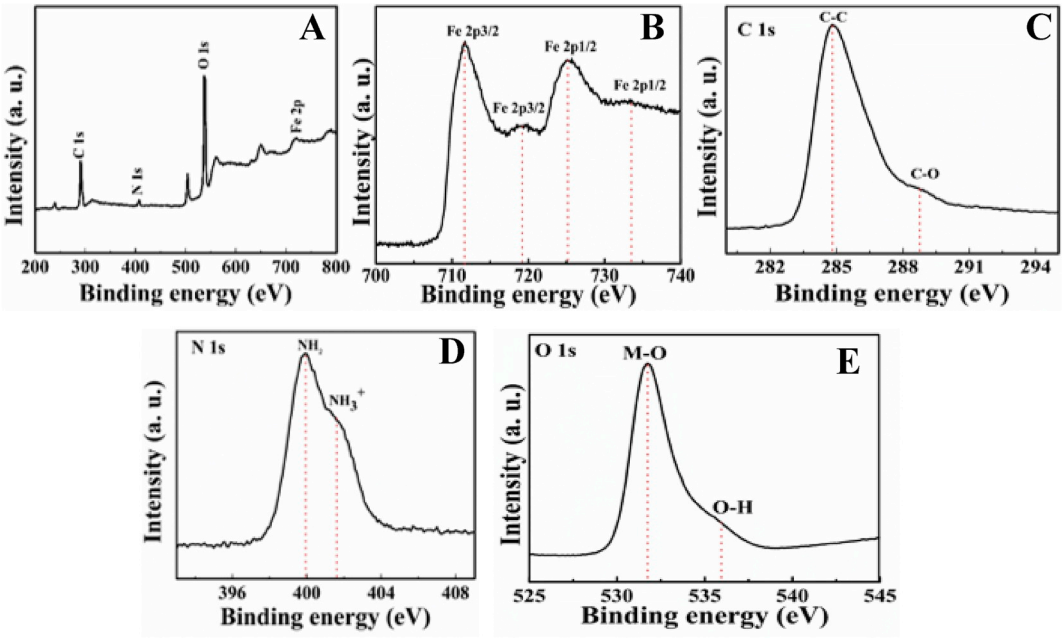

Fig. 4. XPS spectra of PANI-Fe_2O_3 composite: (A) Survey scan spectrum, (B–E) high-resolution scan spectra of (B) Fe 2p; (C) C 1s; (D) N 1s and (E) O 1s.

matrix. The width of the rod-shaped particles was at the range of 50–150 nm. Rods with length up to 500 nm was seen. A few spherical agglomerates were also observed. The particle size and crystalline nature of PANI-Fe_2O_3 composite were confirmed from HRTEM analysis (Fig. 2C&D). The light shade in the TEM images represent the polymer backbone, and the black shade represent the Fe_2O_3 particles embedded on the polymer matrix [52]. The d spacing of 0.21 nm could be attributed to (110) plane of α-Fe_2O_3 [53]. The different magnifications of FESEM and HRTEM images are provided in the supporting information (Fig. S_1 and Fig. S_2, Supporting Information).

EDS analysis of elemental composition further confirmed the compositional purity and the existence of C, N, O and Fe in the composite, and the elemental distribution as evidenced by the mapping studies (Fig. 3).

Surface elemental composition of the composites was confirmed by XPS analysis (Fig. 4). XPS survey spectrum of the composite exhibited the presence of Fe 2p, C 1s, N 1s, and O 1s core levels with no evidence of impurities [54–56]. The XPS peak at 712 eV and 725 eV corresponds to

Table 1
Comparison of roughness parameters of various compositions of PANI-Fe_2O_3-alkyd resin coatings.

Coating	S_a (μm)	S_q (μm)	S_p (μm)	S_v (μm)	S_t (μm)	S_{sk} (μm)	S_{ku} (μm)
Bare alkyd resin	4.34	5.39	37.78	−43.1	79.4	0.82	2.87
PANI-Fe_2O_3 1(g/L)/alkyd resin	4.25	5.33	32.14	−33.82	65.96	0.52	2.76
PANI-Fe_2O_3 2(g/L)/alkyd resin	3.39	4.24	23.62	−22.68	61.74	0.43	2.53
PANI-Fe_2O_3 5(g/L) /alkyd resin	3.94	5.47	31.58	−26.68	67.58	0.53	2.75
PANI-Fe_2O_3 10(g/L)/alkyd resin	4.53	4.88	33.7	−29.9	67.7	0.62	2.84

Fe2p3/2 and Fe2p1/2, and that revealed that Fe exists in different oxidation states in the composite. The peak at 712 eV is due to the presence of Fe in +2 oxidation state, and the peak at 725 eV corresponds to the higher oxidation state. Each peak possessed a spin-orbit coupling component (Fe2p3/2–719.8 eV, Fe2p1/2–734.7 eV) [56]. C 1s spectrum exhibited two peaks, the strong peak at 284.9 eV is associated with the C=C bond, whereas the shoulder peak at 288.5 eV can be associated with the C–O bond. The later can be an indication of the effective interaction of metal oxide with the polymer matrix [54,55]. The O 1s spectrum exhibited one strong peak corresponding to Fe–O bond at 532 eV and a shoulder peak at 536 eV corresponding to O–H group. N 1s spectrum exhibited two peaks at 400 eV and 401.8 eV corresponding to amino –NH– and protonated amino group, respectively.

The TGA plot of the PANI-Fe_2O_3 composite is shown in Fig. S_3 (Supporting Information). The plot revealed two major weight loss regions. The first region starts at 200 °C and the second one at 400 °C. The weight loss at 200 °C could be attributed to the elimination of ammonia, moisture and other volatile compounds associated with the polymer. The degradation at 400 °C can be attributed to the high-temperature decomposition of the polymer backbone. The good stability of the fabricated composite (up to 400 °C) is evident from the TGA plot.

3.2. Characterization of PANI-Fe_2O_3 composite-incorporated alkyd coating

The topography of the coatings could be studied from OSP analysis. The valleys and peaks in the polymer alkyd resin coating represent the roughness intensity of the surface. The surface profilograms of different coatings are represented in Fig. S_4 (Supporting Information) where different roughness parameters such as S_a, S_q, S_p, S_v, S_t, S_{ku}, S_{sk} etc. are extracted from the profilometry (Table 1). S_a values indicate the arithmetic average height of peaks and valleys in the coating. All the coatings exhibited low S_a values revealing better corrosion resistant characteristics. The lowest value was recorded for a 2 g/L PANI-Fe_2O_3 incorporated coating. The variation of root mean square roughness, S_q can be taken as a relative measure of protective nature of coatings; the minimum surface roughness indicates a more corrosion resistant nature. From Table 1, it is clear that Sq values reduced significantly for most of the composite coatings. The surface kurtosis value, S_{ku} of all the coatings is less than 3, and that also denotes lack of peaks and valleys. The degree of symmetry of surface heights about the mean plane is represented by S_{sk}; a low skewness value near to zero indicates better surface smoothness. Other parameters considered in the study are maximum peak height of the areal surface (S_p), maximum valley depth of the area surface (S_v), and maximum peak to valley height of areal surface (S_t). These parameters also provide valuable information on coating topography; the coating thickness was found to be in the range of 60–80 μm [57,58]. The study thus indicates that incorporation of PANI-Fe_2O_3 composite to the alkyd resin coating was beneficial to increase the surface smoothness. The PANI-Fe_2O_3 2(g/L)/alkyd resin coating showed the best results.

SKPM is a non-destructive and non-contact method which gives information regarding the corrosion susceptibility of an electrode via surface potential measurement. The measured potential of the electrode is related to its corrosion potential [35,59]. The 2D and 3D SKPM images of various compositions of PANI-Fe_2O_3 incorporated alkyd resin coatings are shown in Fig. 5. The highest and lowest Volta potentials associated with the bare alkyd resin coating are −0.52 V and −0.34 V respectively. On incorporation of PANI-Fe_2O_3 composite to the bare alkyd resin, a distinct change in the potential could be observed. The higher Volta potential shifted to −0.90, −0.62, −0.52 and −0.58 V for 1, 2, 5 and 10 g/L PANI-Fe_2O_3 composite to the coating whereas the corresponding lower Volta potential shifted to −0.78, −0.52, −0.40 and −0.44 V. The Volta potential shift (ΔV) shown by the bare alkyd resin, PANI-Fe_2O_3 1(g/L)/alkyd resin, PANI-Fe_2O_3 2(g/L)/alkyd resin, PANI-Fe_2O_3 5(g/L)/alkyd resin, and PANI-Fe_2O_3 10(g/L)/alkyd resin

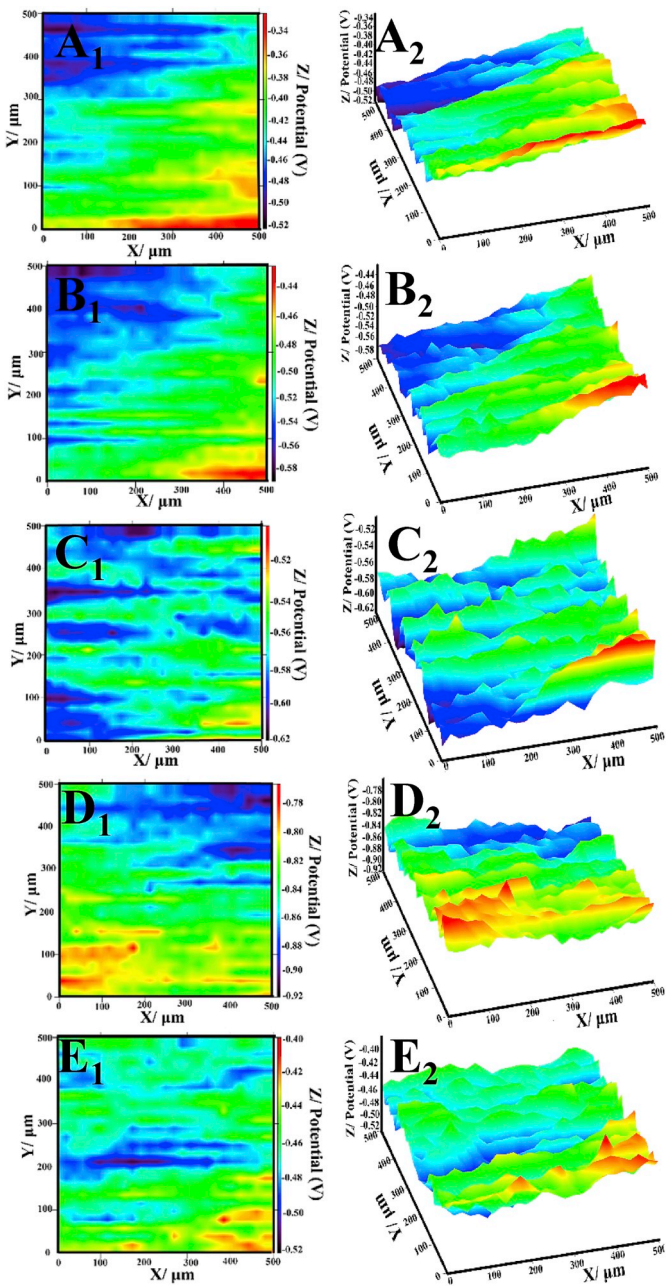

Fig. 5. The two dimensional and three dimensional SKPM images of (A) Bare alkyd, (B) PANI-Fe_2O_3 1(g/L)/alkyd, (C) PANI-Fe_2O_3 2(g/L)/alkyd, (D) PANI-Fe_2O_3 5(g/L)/alkyd, and (E) PANI- Fe_2O_3 10(g/L)/alkyd resin coatings.

coatings are 0.18, 0.12, 0.10, 0.12 and 0.14 V respectively. The lowest ΔV is exhibited by the 2(g/L) PANI-Fe_2O_3 incorporated alkyd coating, and that could be due to a more uniform smooth coating resulted with better adhesion to the surface.

The SEM surface view images of the bare alkyd and 0.02 g PANI-Fe_2O_3 composite-incorporated alkyd coating in different magnifications are shown in Fig. 6. In the bare alkyd coating, the particles are observed to be scattered on the surface, and that may result in a rough surface. However, the surface appeared more compact, smooth and rigid in the case of PANI-Fe_2O_3 composite-incorporated alkyd resin coating. A smooth and compact surface can effectively prevent the penetration of the corrosive species to the metal/solution interface. Corresponding EDS spectra are also shown in Fig. 6 that confirms successful incorporation of PANI and Fe_2O_3 in the coating. EDS mapping (Fig. 7) evidences the uniform distribution of the elements in the coating. The average coating

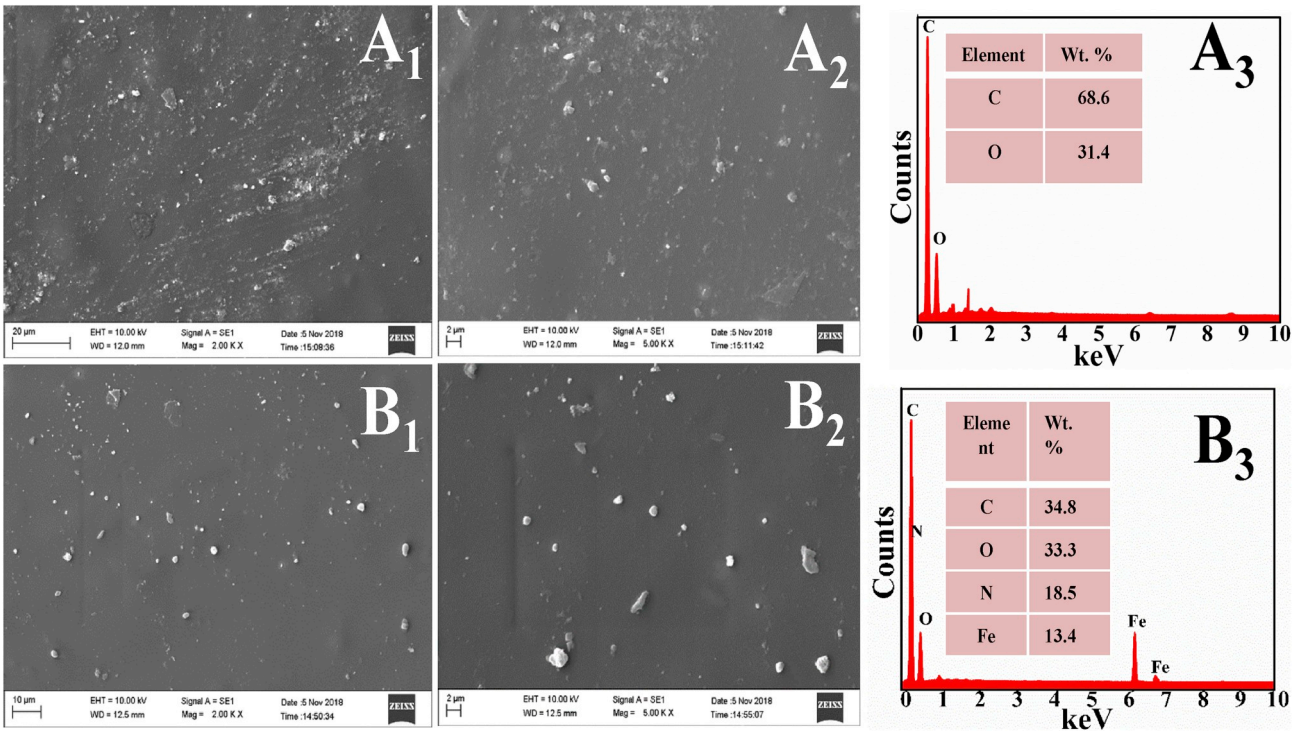

Fig. 6. SEM and EDS analysis of (A) alkyd resin coating, and (B) PANI-Fe_2O_3 2(g/L)/alkyd resin coating.

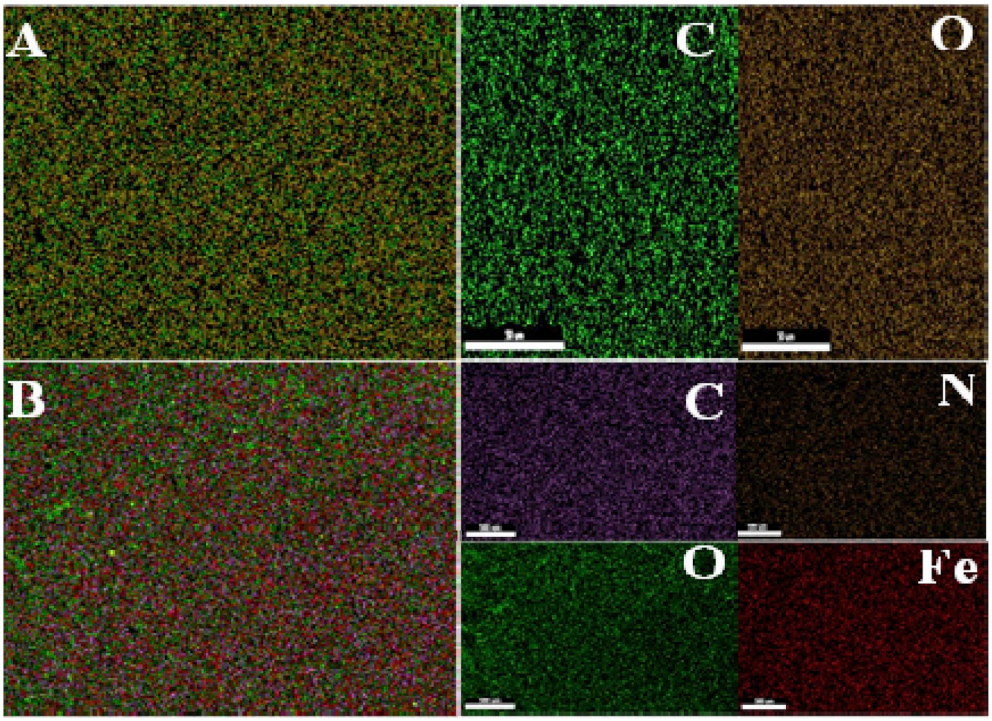

Fig. 7. EDS mapping of A) alkyd resin coating, and B) PANI-Fe_2O_3 2(g/L)/alkyd resin coating. The corresponding elemental mapping of C, N, O and Fe are also provided.

thickness as measured from SEM cross sectional image was ~70 μm (Fig. S_5, Supporting Information).

3.3. Electrochemical corrosion studies

Potentiodynamic polarization studies were carried out in acidic and neutral chloride solutions for determining the anticorrosion property. Anodic (β_a) and cathodic (β_c) Tafel slopes were obtained by polarization curve fitting, and the polarization resistance (R_p) calculated using the Stern-Geary equation (Eq. (1)) [60,61]. The corrosion rate (C_R) was calculated by Eq. (2):

$$R_p = [\beta_a \beta_c / 2.303 (\beta_a + \beta_c)]1/ i_{corr} \quad (1)$$

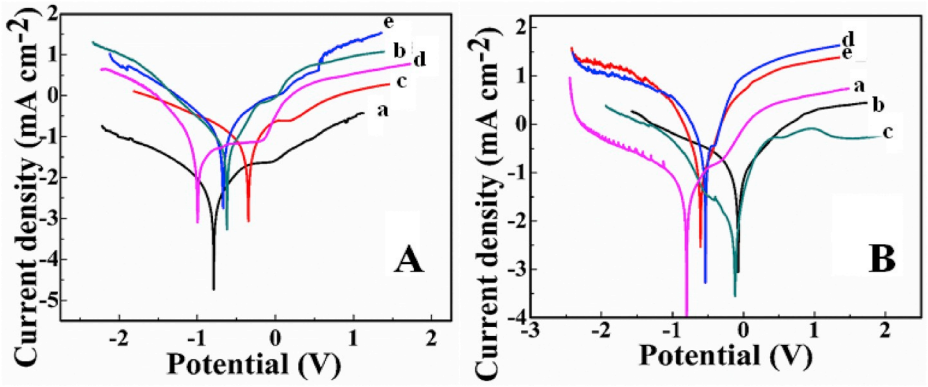

Fig. 8. Tafel polarization curves of different compositions of PANI-Fe_2O_3/alkyd resin in (A) 3.5% NaCl, and (B) 1 M HCl. Plots of (a) bare alkyd (b) PANI- Fe_2O_3 1(g/L)/alkyd (c) PANI- Fe_2O_3 2(g/L)/alkyd (d) PANI- Fe_2O_3 5(g/L)/alkyd, and (e) PANI- Fe_2O_3 10(g/L)/alkyd resin coated steel are provided.

Table 2
Polarization and EIS parameters of PANI-Fe_2O_3-alkyd resin coatings in 3.5% NaCl.

Type of coating	β_a (V/dec)	β_c (V/dec)	E_{corr} (V)	i_{corr} ($\mu A/cm^2$)	R_p (KΩ cm^2)	C_R (mmpy)	R_s (Ohm cm^2)	R_{ct} (Ohm cm^2)	C_{dl} (μ F/cm^2)
Bare alkyd resin	0.322	0.373	−0.345	56.88	10.53	0.123	29.03	1514	428
PANI-Fe2O3 1(g/L)/alkyd resin	0.279	0.357	−0.610	29.24	12.33	0.095	633.30	6704	21.56
PANI- Fe_2O_3 2(g/L)/alkyd resin	0.295	0.285	−0.962	1.80	185.46	0.006	2560	9380	5.26
PANI- Fe_2O_3 5(g/L)/alkyd resin	0.442	0.233	−0.783	20.613	17.04	0.067	0.212	2003	11.43
PANI- Fe_2O_3 10(g/L)/alkyd resin	0.298	0.308	−0.677	37.79	6.13	0.186	45.40	2778	24.15
PANI/alkyd resin	0.275	0.291	−0.547	24.36	13.36	0.197	1247	2458	34.57

Table 3
Polarization and EIS parameters of PANI-Fe_2O_3-alkyd resin coatings in 1 M HCl.

Type of coating	β_a (V/dec)	β_c (V/dec)	E_{corr} (V)	i_{corr} ($\mu A/cm^2$)	R_p (KΩ cm^2)	C_R (mmpy)	R_s (Ohm cm^2)	R_c (Ohm cm^2)	R_{ct} (Ohm cm^2)	C_c ($\mu F/cm^2$)	C_{dl} ($\mu F/cm^2$)
Bare alkyd resin	0.316	0.242	−0.079	165.18	1.913	0.542	2101	39.68	1225	11.11	82.58
PANI-Fe_2O_3 1(g/L)/alkyd resin	0.283	0.308	−0.129	41.65	8.155	0.136	18.80	201.2	6627	0.88	7.62
PANI- Fe_2O_3 2(g/L)/alkyd resin	0.170	0.395	−0.791	6.25	43.794	0.020	1122	38019	33635	0.01	0.01
PANI- Fe_2O_3 5(g/L)/alkyd resin	0.188	0.262	−0.581	80.13	3.146	0.262	29.93	286.7	7421	42.93	3.75
PANI- Fe_2O_3 10(g/L)/alkyd resin	0.340	0.349	−0.531	22.76	17.426	0.074	79.85	1523	1393	77.04	10.46
PANI/alkyd resin	0.312	0.298	−0.421	90.24	3.88	0.184	1247	745	2184	56.18	54.87

$$C_R = K\ (i_{corr}/\rho)\ EW \quad (2)$$

Where $K = 3.27 \times 10^{-3}$, ρ is the density and EW is the equivalent weight of the substrate.

The Tafel polarization curves in 3.5% NaCl are shown in Fig. 8A and the corresponding electrochemical parameters are provided in Table 2. The i_{corr} decreased significantly on the addition of PANI-Fe_2O_3 composite to the alkyd coating. The recoded i_{corr} values are 56.88, 29.24, 1.80, 20.61 and 37.79 $\mu A\ cm^{-2}$ respectively for the bare alkyd, PANI-Fe_2O_3 1(g/L)/alkyd, PANI-Fe_2O_3 2(g/L)/alkyd, PANI-Fe_2O_3 5(g/L)/alkyd and PANI-Fe_2O_3 10(g/L)/alkyd resin coatings. The low i_{corr} and the least C_R obtained for the PANI-Fe_2O_3 2(g/L)/alkyd resin coating was in accordance with the OSP, SKPM and SEM studies. The equivalent E_{corr} values are −0.610, −0.345, −0.962, −0.783 and −0.677 V. The positive shift of E_{corr} of PANI-Fe_2O_3 1(g/L)/alkyd coating indicates the predominant anodic protection of the incorporated PANI. However, for PANI-Fe_2O_3 2(g/L)/alkyd, a more negative E_{corr} was obtained, and that can be due to the effective filling of the coating pores by the incorporated Fe_2O_3. With further increase of the composite content, it is expected that a higher non-uniformity occurs due to agglomeration resulting in a lower barrier protection. The highest R_p value calculated (185.46 KΩ) corresponds to the PANI-Fe_2O_3 2(g/L)/alkyd coating. The Tafel plots of the coated steel in 1 M HCl (Fig. 8B and Table 3) displayed a similar variation where the PANI-Fe_2O_3 2(g/L)/alkyd coating displayed the lowest i_{corr} (6.25 $\mu A\ cm^{-2}$) and the highest E_{corr} (−0.791 V) values. The C_R calculated was 0.020 mmpy (Table 3).

The corrosion parameters provided in Tables 2 and 3 confirm that the higher corrosion resistance of the PANI-Fe_2O_3 2(g/L)/alkyd coating is mainly attributed to the Fe_2O_3 filler. It is also observed that the composite coating performed better in the acidic medium than in neutral chloride medium. This can be explained by the possibility that in the acidic medium an exposed iron surface at the pinholes can be protected by the complementary cathodic reaction of the conductive emaraldene PANI to the nonconductive leuco PANI. But in a neutral medium, such counter-reactions are not possible. Also, the sudden ingression of hydrogen to the interface can result in an instantaneous corrosion, and the resulting corrosion products can effectively fill the pores, and that can restrict the further entry of the aggressive species. Tafel extrapolation method, however, can be erratic in determining the corrosion rates of coated metals as the active area is unknown and the corrosion may eventually get localized. However, our impedance studies also revealed a similar behavior where a higher charge transfer resistance (R_{ct}) was always recorded for the PANI-Fe_2O_3 2(g/L)/alkyd coated steel.

EIS is the preferable method for studying the corrosion-resistant characteristics of the organic coatings [62–64]. Nyquist and Bode plots of different compositions of PANI-Fe_2O_3/alkyd resin coatings in 3.5% NaCl and 1 M HCl are provided in Fig. 9 and Fig. 10, respectively. The equivalent circuit used to fit the plots are given in Fig. 11. The circuit contains three resistance parameters, namely solution resistance

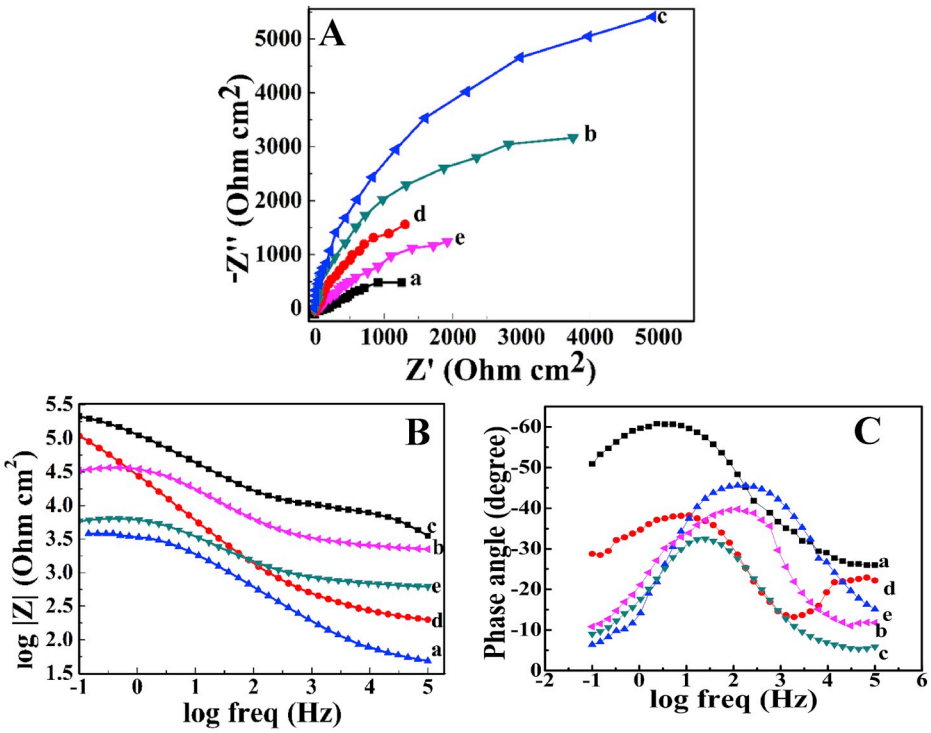

Fig. 9. A) Nyquist, B) Bode impedance, and C) Bode phase angle plots of different compositions of PANI-Fe_2O_3/alkyd resin coating (a) Bare alkyd, (b) PANI-Fe_2O_3 1 (g/L)/alkyd, (c) PANI-Fe_2O_3 2(g/L)/alkyd, (d) PANI-Fe_2O_3 5(g/L)/alkyd, and (e) PANI-Fe_2O_3 10(g/L)/alkyd resin coatings in 3.5% NaCl solution at 298 K.

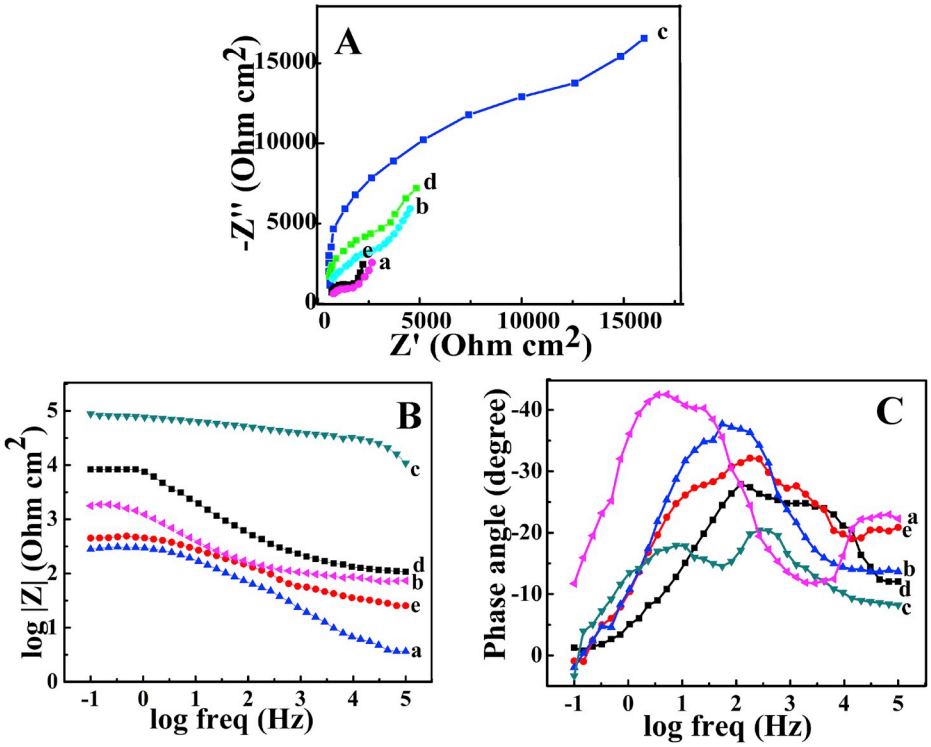

Fig. 10. A) Nyquist plots, B) Bode impedance, and C) Bode phase angle plots of different compositions of PANI-Fe_2O_3/alkyd resin coating (a) Bare alkyd, (b) PANI-Fe_2O_3 1(g/L)/alkyd, (c) PANI-Fe_2O_3 2(g/L)/alkyd, (d) PANI-Fe_2O_3 5(g/L)/alkyd, and (e) PANI-Fe_2O_3 10(g/L)/alkyd resin coatings in 3.5% NaCl solution at 298 K.

(R_s), coating pore resistance (R_c) and charge transfer resistance (R_{ct}). C_c is the capacitance of the coating and C_{dl} the double layer capacitance. Tables 2 and 3 show the corresponding fit parameters.

The Nyquist plots of coated samples exhibit one-time constant in NaCl (Fig. 9A) and two-time constants in HCl (Fig. 10A). This is more evident from the corresponding Bode phase angle plots in NaCl (Fig. 9 B&C) and HCl (Fig. 10 B&C). The first time constant is attributed to the coating characteristics and the second time constant to the charge

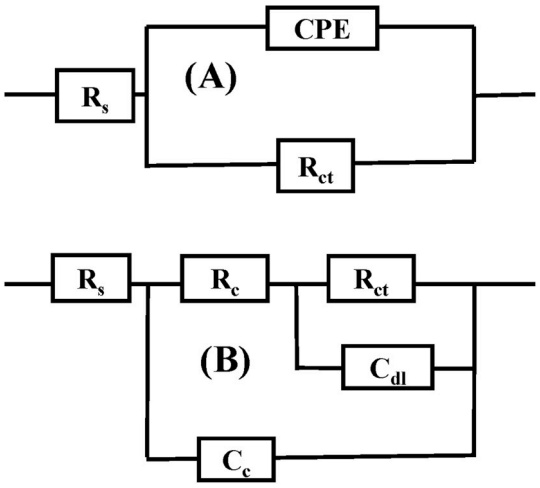

Fig. 11. Equivalent circuit diagram used for coatings in (A) 3.5% NaCl, and (B) 1 M HCl.

transfer reactions occurring at the interface. The highest semicircle diameter and the highest R_{ct} values were always obtained for the PANI-Fe_2O_3 2(g/L)/alkyd coating showing better corrosion resistant characteristics [65–68]. The decreased R_{ct} with an increasing amount of PANI-Fe_2O_3 in the coating may be due to the potential agglomeration issues in the nanocomposite coating.

The best performance of PANI-Fe_2O_3 2(g/L)/alkyd resin coating is evident from Tables 2 and 3 The optimized composite coating showed higher R_c values in the acidic medium than in neutral chloride medium. This could be mainly attributed to the complementary cathodic reaction of the conductive emeraldine-PANI in acidic medium forming the nonconductive leuco-PANI, as discussed above. The effective blockage of the coating defects by the initially formed corrosion products can also contribute. The two-time constant behavior and the higher R_c values of the PANI-Fe_2O_3 2(g/L)/alkyd coated steel are supportive evidence. The larger impedance values support the fact that the formed corrosion products successfully prevented further ingression of aggressive species and maintained a higher corrosion resistance property.

The better corrosion resistance of PANI-Fe_2O_3/2(g/L)/alkyd coating is also evident from the higher impedance and the lower phase angle values in the Bode plots. The higher C_c of the bare alkyd coating can be attributed to the increased water absorption. This is associated with the higher relative permittivity of water (80) when compared to that of typical organic resins whose relative permittivity lies at the range of 2.5–10. The compact PANI-Fe_2O_3/alkyd resin coating prevents the penetration of water and corrosive species more effectively producing improved barrier protection.

The mechanism of corrosion inhibition depends upon the nature of substrate, electrolyte and coating composition [69]. Corrosion protection associated with organic coating can be mainly attributed to the barrier protection. Herein PANI- Fe_2O_3/alkyd resin coating, the corrosion prevention is due to the combined effect of barrier protection of polymer matrix in the coating and the corrosion inhibiting polar functionalities of the PANI. The polar functionalities in the coating provide strong interaction between the coating and the metal surface leading to the formation of a compact and tightly adhered coating. The Fe_2O_3 nanoparticles act as a filler and provide a locking effect between the cracks and the voids present in the coating [70].

3.4. Open circuit potential (OCP) measurement

The long-term stability of PANI-Fe_2O_3/alkyd resin coatings is evaluated by OCP decay measurements up to 30 days (Fig. 12 A&B). The OCP values showed a gradual decrease in both NaCl and HCl, conceivably due to the continuous ingression of the electrolyte species to the metal/solution interface and that can be attributed to the defects in the lab-made coating as well as the highly aggressive solutions used. The

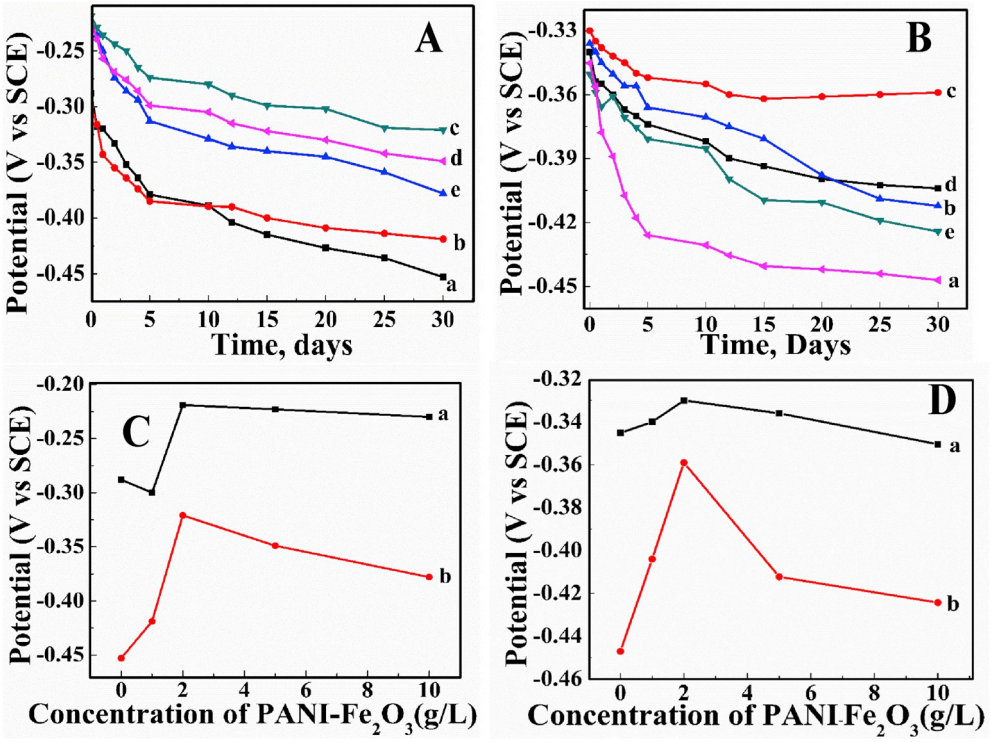

Fig. 12. OCP variation as a function of immersion time of PANI- Fe_2O_3/alkyd resin coatings in (A) 3.5% NaCl, and (B) 1 M HCl: (a) Bare alkyd, (b) 1(g/L)/alkyd, (c) PANI-Fe_2O_3 2(g/L)/alkyd, (d) PANI-Fe_2O_3 5(g/L)/alkyd, and (e) PANI-Fe_2O_3 10(g/L)/alkyd resin coatings. (C & D) OCP variation as a function of concentration of PANI-Fe_2O_3 in the coating at (a) immediately after initial immersion and (b) after 30 days of immersion in 3.5% NaCl and 1 M HCl respectively.

PANI-Fe_2O_3 2(g/L)/alkyd coating showed the lowest cathodic shift of OCP.

More noble values of OCP were always recorded with PANI-Fe_2O_3 2 (g/L)/alkyd coating (Fig. 12C&D). The coating maintained a stable and acceptable range of OCP values even after 30 days. The bare alkyd resin coating showed the most negative potential shift displaying lesser stability with time.

4. Conclusions

PANI-Fe_2O_3 nanocomposite was synthesized by a novel *in situ* polymerization technique and characterized for phase, microstructure, compositional purity and stability. The composite was incorporated into a commercial alkyd resin and developed an efficient anticorrosive coating for mild steel. The surface smoothness and uniformity of the composite-incorporated coating were confirmed by surface profilometric and morphological analysis. Electrochemical studies showed that the PANI-Fe_2O_3/alkyd resin coating provided better corrosion protection to mild steel in comparison to conventional alkyd resin coating and that is attributed to the higher passivation ability and the filler effect of PANI-Fe_2O_3. 2 (g/L) PANI-Fe_2O_3 incorporated alkyd resin coating proved to be the best anticorrosive coating. The present approach hence provided a way to develop environmentally friendly conducting polymer-metal oxide-alkyd resin coatings with improved anticorrosion capabilities.

Declaration of competing interest

The authors declare that they have no known competing financial interests or personal relationships that could have appeared to influence the work reported in this paper.

Acknowledgement

The authors acknowledge The Head, Department of Chemistry and CLIF, University of Kerala, Kariavattom, Thiruvananthapuram for providing facilities for this work and also thankful to University Grant Commission for availing fellowship.

Appendix A. Supplementary data

Supplementary data to this article can be found online at https://doi.org/10.1016/j.matchemphys.2020.122881.

References

[1] Z. Mirzakhanzadeh, A. Kosari, M.H. Moayed, R. Naderi, P. Taheri, J.M.C. Mol, Enhanced corrosion protection of mild steel by the synergetic effect of zinc aluminum polyphosphate and 2-mercaptobenzimidazole inhibitors incorporated in epoxy-polyamide coatings, Corrosion Sci. 138 (2018) 372–379.
[2] M.T.O. Jonker, S.A. van der Heijden, D. Adelman, J.N. Apell, R.M. Burgess, Y. Choi, L.A. Fernandez, G.M. Flavetta, U. Ghosh, P.M. Gschwend, S.E. Hale, M. Jalalizadeh, M. Khairy, M.A. Lampi, W. Lao, R. Lohmann, M.J. Lydy, K.A. Maruya, S.A. Nutile, A.M.P. Oen, M.I. Rakowska, D. Reible, T.P. Rusina, F. Smedes, Y. Wu, Advancing the use of passive sampling in risk assessment and management of contaminated sediments: results of an international passive sampling inter-laboratory comparison, Environ. Sci. Technol. 52 (2018) 3574–3582.
[3] M.A. Deyab, R. Słota, E. Bloise, G. Mele, Exploring corrosion protection properties of alkyd@ lanthanide bis-phthalocyanine nanocomposite coatings, RSC Adv. 8 (2018) 1909–1916.
[4] O. ur Rahman, S. Ahmad, Physico-mechanical and electrochemical corrosion behavior of soy alkyd/Fe 3 O 4 nanocomposite coatings, RSC Adv. 4 (2014) 14936–14947.
[5] Z. Ding, F. Fatollahi-Fard, I.S. Kwon, P.C. Pistorius, C.J. Bettinger, Polydopamine nanomembranes as adhesion layers for improved corrosion resistance in low carbon steel, Adv. Eng. Mater. 20 (2018) 1800621.
[6] J.I.I. Laco, F.C. Villota, F.L. Mestres, Corrosion protection of carbon steel with thermoplastic coatings and alkyd resins containing polyaniline as conductive polymer, Prog. Org. Coating 52 (2005) 151–160.
[7] B.A. Bhanvase, S.H. Sonawane, New approach for simultaneous enhancement of anticorrosive and mechanical properties of coatings: application of water repellent nano CaCO3–PANI emulsion nanocomposite in alkyd resin, Chem. Eng. J. 156 (2010) 177–183.
[8] S. Pathan, S. Ahmad, Green and sustainable anticorrosive coating derived from waterborne linseed alkyd using organic-inorganic hybrid cross linker, Prog. Org. Coating 122 (2018) 189–198.
[9] M.S. Selim, S.A. El-Safty, M.A. Shenashen, M.A. El-Sockary, O.M.A. Elenien, A. M. El-Saeed, Robust alkyd/exfoliated graphene oxide nanocomposite as a surface coating, Prog. Org. Coating 126 (2019) 106–118.
[10] S. Zheng, J. Li, Inorganic–organic sol gel hybrid coatings for corrosion protection of metals, J. Sol. Gel Sci. Technol. 54 (2010) 174–187.
[11] U. Riaz, C. Nwaoha, S.M. Ashraf, Recent advances in corrosion protective composite coatings based on conducting polymers and natural resource derived polymers, Prog. Org. Coating 77 (2014) 743–756.
[12] O. ur Rahman, M. Kashif, S. Ahmad, Nanoferrite dispersed waterborne epoxy-acrylate: anticorrosive nanocomposite coatings, Prog. Org. Coating 80 (2015) 77–86.
[13] P. Herrasti, F.J. Recio, P. Ocon, E. Fatás, Effect of the polymer layers and bilayers on the corrosion behaviour of mild steel: comparison with polymers containing Zn microparticles, Prog. Org. Coating 54 (2005) 285–291.
[14] M. Ates, A review on conducting polymer coatings for corrosion protection, J. Adhes. Sci. Technol. 30 (2016) 1510–1536.
[15] R. Figueira, I. Fontinha, C. Silva, E. Pereira, Hybrid sol-gel coatings: smart and green materials for corrosion mitigation, Coatings 6 (2016) 12.
[16] X. Sheng, W. Cai, L. Zhong, D. Xie, X. Zhang, Synthesis of functionalized graphene/polyaniline nanocomposites with effective synergistic reinforcement on anticorrosion, Ind. Eng. Chem. Res. 55 (2016) 8576–8585.
[17] K. Saravanan, S. Sathiyanarayanan, S. Muralidharan, S.S. Azim, G. Venkatachari, Performance evaluation of polyaniline pigmented epoxy coating for corrosion protection of steel in concrete environment, Prog. Org. Coating 59 (2007) 160–167.
[18] L. Ejenstam, A. Swerin, J. Pan, P.M. Claesson, Corrosion protection by hydrophobic silica particle-polydimethylsiloxane composite coatings, Corrosion Sci. 99 (2015) 89–97.
[19] E. Zumelzu, H.G. de Melo, A.R. Di Sarli, C.R. Tomachuk, Effect of passivation treatment on adhesion and protective properties of steel coated with polymeric film, Mater. Sci. Forum 930 (2018) 422–427.
[20] S. Qiu, C. Chen, W. Zheng, W. Li, H. Zhao, L. Wang, Long-term corrosion protection of mild steel by epoxy coating containing self-doped polyaniline nanofiber, Synth. Met. 229 (2017) 39–46.
[21] M.L. Zheludkevich, J. Tedim, M.G.S. Ferreira, 'Smart' coatings for active corrosion protection based on multi-functional micro and nanocontainers, Electrochim. Acta 82 (2012) 314–323.
[22] A.F. Baldissera, C.A. Ferreira, Coatings based on electronic conducting polymers for corrosion protection of metals, Prog. Org. Coating 75 (2012) 241–247.
[23] G.S. Gonçalves, A.F. Baldissera, L.F. Rodrigues Jr., E.M.A. Martini, C.A. Ferreira, Alkyd coatings containing polyanilines for corrosion protection of mild steel, Synth. Met. 161 (2011) 313–323.
[24] C. Ocampo, E. Armelin, F. Liesa, C. Alemán, X. Ramis, J.I. Iribarren, Application of a polythiophene derivative as anticorrosive additive for paints, Prog. Org. Coating 53 (2005) 217–224.
[25] M.Z. Hussain, S. Khan, S. Haque, B. Pathak, Review of synthesis, characterization, mechanical and electrical properties of CNTs/PANI nanocomposite, Int. J. 5 (2017) 440–443.
[26] V. Kumar, T. Yokozeki, T. Goto, T. Takahashi, Synthesis and characterization of PANI-DBSA/DVB composite using roll-milled PANI-DBSA complex, Polymer 86 (2016) 129–137.
[27] B.A. Bhanvase, S.H. Sonawane, Ultrasound assisted in situ emulsion polymerization for polymer nanocomposite: a review, Chem. Eng. Process. Process Intensif. 85 (2014) 86–107.
[28] A.K. Gaharwar, N.A. Peppas, A. Khademhosseini, Nanocomposite hydrogels for biomedical applications, Biotechnol. Bioeng. 111 (2014) 441–453.
[29] V. Karpakam, K. Kamaraj, S. Sathiyanarayanan, G. Venkatachari, S. Ramu, Electrosynthesis of polyaniline–molybdate coating on steel and its corrosion protection performance, Electrochim. Acta 56 (2011) 2165–2173.
[30] S. Radhakrishnan, C.R. Siju, D. Mahanta, S. Patil, G. Madras, Conducting polyaniline–nano-TiO2 composites for smart corrosion resistant coatings, Electrochim. Acta 54 (2009) 1249–1254.
[31] S. Shi, Z. Zhang, L. Yu, Hydrophobic polyaniline/modified SiO2 coatings for anticorrosion protection, Synth. Met. 233 (2017) 94–100.
[32] S. Liu, L. Liu, H. Guo, E.E. Oguzie, Y. Li, F. Wang, Electrochemical polymerization of polyaniline-reduced graphene oxide composite coating on 5083 Al alloy: Role of reduced graphene oxide, Electrochem. Commun. 98 (2019) 110–114.
[33] S. Sathiyanarayanan, S.S. Azim, G. Venkatachari, Preparation of polyaniline–Fe2O3 composite and its anticorrosion performance, Synth. Met. 157 (2007) 751–757.
[34] M. Kryszewski, J.K. Jeszka, Nanostructured conducting polymer composites—superparamagnetic particles in conducting polymers, Synth. Met. 94 (1998) 99–104.
[35] T. Sun, H. Fan, Z. Wang, X. Liu, Z. Wu, Modified nano Fe2O3-epoxy composite with enhanced mechanical properties, Mater. Des. 87 (2015) 10–16.
[36] Y. Wang, X. Jing, Intrinsically conducting polymers for electromagnetic interference shielding, Polym. Adv. Technol. 16 (2005) 344–351.
[37] D.E. Tallman, Y. Pae, G.P. Bierwagen, Conducting polymers and corrosion: polyaniline on steel, Corrosion 55 (1999) 779–786.

[38] A. Zhu, H. Wang, S. Sun, C. Zhang, The synthesis and antistatic, anticorrosive properties of polyaniline composite coating, Prog. Org. Coating 122 (2018) 270–279.
[39] S. Khasim, S.C. Raghavendra, M. Revanasiddappa, K.C. Sajjan, M. Lakshmi, M. Faisal, Synthesis, characterization and magnetic properties of polyaniline/γ-Fe 2 O 3 composites, Bull. Mater. Sci. 34 (2011) 1557–1561.
[40] L. Wu, Y. Ge, L. Zhang, D. Yu, M. Wu, H. Ni, Enhanced electrical conductivity and competent mechanical properties of polyaniline/polyacrylate (PANI/PA) composites for antistatic finishing prepared at the aid of polymeric stabilizer, Prog. Org. Coating 125 (2018) 99–108.
[41] T. Schauer, A. Joos, L. Dulog, C.D. Eisenbach, Protection of iron against corrosion with polyaniline primers, Prog. Org. Coating 33 (1998) 20–27.
[42] Y. Chen, X.H. Wang, J. Li, J.L. Lu, F.S. Wang, Long-term anticorrosion behaviour of polyaniline on mild steel, Corrosion Sci. 49 (2007) 3052–3063.
[43] S.G. Pawar, S.L. Patil, M.A. Chougule, S.N. Achary, V.B. Patil, Microstructural and optoelectronic studies on polyaniline: TiO2 nanocomposites, Int. J. Polym. Mater. 60 (2010) 244–254.
[44] S.G. Pawar, S.L. Patil, M.A. Chougule, B.T. Raut, S. Sen, V.B. Patil, Camphor sulfonic acid doped polyaniline-titanium dioxide nanocomposite: synthesis, structural, morphological, and electrical properties, Int. J. Polym. Mater. 60 (2011) 979–987.
[45] T. Sen, N.G. Shimpi, S. Mishra, R. Sharma, Polyaniline/γ-Fe2O3 nanocomposite for room temperature LPG sensing, Sensor. Actuator. B Chem. 190 (2014) 120–126.
[46] L. Chen, Q. Xiong, W. Li, J. Li, X. Yu, A solvothermal transformation of α-Fe 2 O 3 nanocrystals to Fe 3 O 4 polyhedrons, CrystEngComm 17 (2015) 8602–8606.
[47] D.K. Bandgar, S.T. Navale, S.A. Vanalkar, J.H. Kim, N.S. Harale, P.S. Patil, V. B. Patil, Synthesis, structural, morphological, compositional and electrical transport properties of polyaniline/α-Fe2O3 hybrid nanocomposites, Synth. Met. 195 (2014) 350–358.
[48] R. Geethanjali, S. Subhashini, Synthesis of magnetite-containing polyaniline–polyacrylamide nanocomposite, characterization and corrosion inhibition behavior on mild steel in acid media, Chem. Sci. Trans 2 (2013) 1148–1159.
[49] A.G. Yavuz, A. Gök, Preparation of TiO2/PANI composites in the presence of surfactants and investigation of electrical properties, Synth. Met. 157 (2007) 235–242.
[50] Z.-L. Wang, R. Guo, G.-R. Li, H.-L. Lu, Z.-Q. Liu, F.-M. Xiao, M. Zhang, Y.-X. Tong, Polyaniline nanotube arrays as high-performance flexible electrodes for electrochemical energy storage devices, J. Mater. Chem. 22 (2012) 2401–2404.
[51] H. Baniasadi, A.R. Sa, S. Mashayekhan, F. Ghaderinezhad, Preparation of conductive polyaniline/graphene nanocomposites via in situ emulsion polymerization and product characterization, Synth. Met. 196 (2014) 199–205.
[52] X. Chen, Z. Zhang, X. Li, C. Shi, Hollow magnetite spheres: synthesis, characterization, and magnetic properties, Chem. Phys. Lett. 422 (2006) 294–298.
[53] Y. Li, H. Zhao, H. Ban, M. Yang, Composites of Fe2O3 nanosheets with polyaniline: Preparation, gas sensing properties and sensing mechanism, Sensor. Actuator. B Chem. 245 (2017) 34–43.
[54] N. Atar, T. Eren, M.L. Yola, H. Karimi-Maleh, B. Demirdögen, Magnetic iron oxide and iron oxide@ gold nanoparticle anchored nitrogen and sulfur-functionalized reduced graphene oxide electrocatalyst for methanol oxidation, RSC Adv. 5 (2015) 26402–26409.
[55] L. Wang, Q. Yao, H. Bi, F. Huang, Q. Wang, L. Chen, PANI/graphene nanocomposite films with high thermoelectric properties by enhanced molecular ordering, J. Mater. Chem. A 3 (2015) 7086–7092.
[56] Y. Huang, Z. Lin, M. Zheng, T. Wang, J. Yang, F. Yuan, X. Lu, L. Liu, D. Sun, Amorphous Fe2O3 nanoshells coated on carbonized bacterial cellulose nanofibers as a flexible anode for high-performance lithium ion batteries, J. Power Sources 307 (2016) 649–656.
[57] M. Sedlaček, B. Podgornik, J. Vižintin, Correlation between standard roughness parameters skewness and kurtosis and tribological behaviour of contact surfaces, Tribol. Int. 48 (2012) 102–112.
[58] S. Bagherifard, D.J. Hickey, S. Fintová, F. Pastorek, I. Fernandez-Pariente, M. Bandini, T.J. Webster, M. Guagliano, Effects of nano features induced by severe shot peening (SSP) on mechanical, corrosion and cytocompatibility properties of magnesium alloy AZ31, Acta Biomater. 66 (2018) 93–108.
[59] A. Nazarov, N. Le Bozec, D. Thierry, Scanning Kelvin Probe assessment of steel corrosion protection by marine paints containing Zn-rich primer, Prog. Org. Coating 125 (2018) 61–72.
[60] Y. Huang, D.K. Sarkar, X.G. Chen, Superhydrophobic aluminum alloy surfaces prepared by chemical etching process and their corrosion resistance properties, Appl. Surf. Sci. 356 (2015) 1012–1024.
[61] M. Cenoui, N. Dkhireche, O. Kassou, M. Ebn Touhami, R. Touir, A. Dermaj, N. Hajjaji, Synergistic influence of molybdate ions with TDMTAA on corrosion inhibition of ordinary steel in cooling water system, J. Mater. Environ. Sci. 1 (2010) 84–95.
[62] S. Sathiyanarayanan, S. Muthukrishnan, G. Venkatachari, D.C. Trivedi, Corrosion protection of steel by polyaniline (PANI) pigmented paint coating, Prog. Org. Coating 53 (2005) 297–301.
[63] V.S. Raja, A. Venugopal, V.S. Saji, K. Sreekumar, S. Nair, M.C. Mittal, Electrochemical impedance behavior graphite dispersed electrically conducting acrylic coating on AZ 31 magnesium alloy in 3.5 wt.% NaCl solution, Prog. Org. Coating 67 (2010) 12–19.
[64] B. Zeybek, E. Aksun, A. Üğe, Investigation of corrosion protection performance of poly (N-methylpyrrole)-dodecylsulfate/multi-walled carbon nanotubes composite coatings on the stainless steel, Mater. Chem. Phys. 163 (2015) 11–23.
[65] J.H. Park, G.D. Lee, A. Nishikata, T. Tsuru, Anticorrosive behavior of hydroxyapatite as an environmentally friendly pigment, Corrosion Sci. 44 (2002) 1087–1095.
[66] A.A.O. Magalhães, I.C.P. Margarit, O.R. Mattos, Electrochemical characterization of chromate coatings on galvanized steel, Electrochim. Acta 44 (1999) 4281–4287.
[67] L. Fedrizzi, F.J. Rodriguez, S. Rossi, F. Deflorian, R. Di Maggio, The use of electrochemical techniques to study the corrosion behaviour of organic coatings on steel pretreated with sol–gel zirconia films, Electrochim. Acta 46 (2001) 3715–3724.
[68] R. Naderi, M.M. Attar, EIS and ENM as tools to evaluate inhibitive performance of second generation of phosphate-based anticorrosion pigments, J. Appl. Electrochem. 39 (2009) 2353–2358.
[69] D.E. Tallman, G. Spinks, A. Dominis, G.G. Wallace, Electroactive conducting polymers for corrosion control, J. Solid State Electrochem. 6 (2002) 73–84.
[70] M. Bagherzadeh, H. Haddadi, M. Iranpour, Electrochemical evaluation and surface study of magnetite/PANI nanocomposite for carbon steel protection in 3.5% NaCl, Prog. Org. Coating 101 (2016) 149–160.